Inorganic Chemistry

pubs.acs.org/IC Article

$Tb_2O@C_2(13333)$-C_{74}: A Non-Isolated Pentagon Endohedral Fullerene Containing a Nearly Linear Tb−O−Tb Unit

James C. Duchamp, Harry C. Dorn,* Aleksander L. Wysocki, Kyungwha Park, Marilyn M. Olmstead, Mrittika Roy, and Alan L. Balch*

Cite This: *Inorg. Chem.* 2023, 62, 5114−5122 Read Online

ACCESS | Metrics & More | Article Recommendations | Supporting Information

ABSTRACT: Terbium has been added to the list of elements that form oxide clusters inside fullerene cages. $Tb_2O@C_2(13333)$-C_{74} has been isolated as a byproduct of the electric arc synthesis of the azafullerene $Tb_2@C_{79}N$. Cocrystallization of $Tb_2O@C_2(13333)$-C_{74} with Ni(OEP) (where OEP is the dianion of octaethylporphyrin) in toluene yielded black needles of $Tb_2O@C_2(13333)$-C_{74}·$Ni^{II}(OEP)$·$1.5C_7H_8$ that have been examined by single-crystal X-ray diffraction. The resulting structure shows that a nearly linear Tb−O−Tb unit is contained in a $C_2(13333)$-C_{74}, which has two sites where pentagons share an edge to form pentalene units at opposite ends of the fullerene. Unlike the usual situations where metal atoms in fullerenes that do not obey the isolated pentagon rule are situated within the folds of the pentalene units, the Tb atoms in $Tb_2O@C_2(13333)$-C_{74} are positioned to the side of the pentalene units and near-neighboring hexagons. The magnetic properties of $Tb_2O@C_2(13333)$-C_{74} have been examined starting from the experimental geometry, using ab-initio multiconfigurational methods. The computations predict that $Tb_2O@C_2(13333)$-C_{74} will show strong axiality, which would make it a single-molecule magnet with a large magnetic anisotropy barrier.

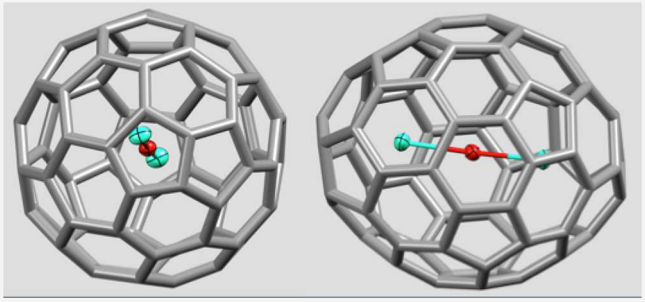

■ INTRODUCTION

Endohedral fullerenes are remarkable molecules that involve a closed carbon cage that acts as a container for individual atoms, molecules, or clusters of atoms.[1−5] In the last case, these clusters have rarely been encountered as identifiable units outside of the endohedral fullerene. These endohedral fullerenes acquire properties that depend upon the atoms trapped inside. Thus, if a paramagnetic metal atom is involved, the retention of its magnetism whilst trapped in the fullerene cage allows it to become useful as a relaxation agent for magnetic resonance imaging (MRI), as is the case with many gadolinium endohedrals.[6−8] Additionally, lutetium-containing endohedrals can act as X-ray contrast agents and may be used as radiopharmaceuticals.[9,10] Other endohedral metallofullerenes have been shown to function as single-molecule magnets.[11−13]

Since the preparation and structural characterization of a case of a metal oxide unit trapped in a fullerene cage, $Sc_4O_2@I_h$-C_{80},[14] several other endohedral fullerenes containing a range of metal-oxo units have been made and characterized.[15,16] For example, endohedral fullerenes have been isolated containing the following scandium oxide clusters: Sc_4O_3 in $Sc_4O_2@I_h$-C_{80},[17] the Sc_4O_2 unit mentioned above, Sc_3O in $Sc_3O@I_h$-C_{80},[18] and Sc_2O in $Sc_2O@C_s(6)$-C_{82}.[19]

Here, we report on the isolation and characterization of $Tb_2O@C_2(13333)$-C_{74}, which is the first endohedral containing a terbium oxide cluster to be identified, crystallographically characterized, and computationally analyzed. The empty cage C_{74} cage has some unusual characteristics. While most empty-cage fullerenes are soluble in solvents such as benzene and carbon disulfide, the C_{74} prepared by arc discharge methods is not soluble in organic solvents and is believed to exist in a polymeric form.[20,21] For empty-cage C_{74}, there is one isomer of D_{3h} symmetry that satisfies the isolated pentagon rule, but that cage has a low calculated highest occupied molecular orbital (HOMO)/lowest unoccupied molecular orbital (LUMO) gap, which is believed to be responsible for its low solubility that results from polymerization of this fullerene. The presence of D_{3h}-C_{74} in carbon soot has been verified by the formation of adducts such as D_{3h}-$C_{74}F_{38}$[22] and C_2-(C_{74}-D_{3h})$(CF_3)_{12}$.[23] Additionally, several endohedral fullerenes have been found to utilize the D_{3h}-C_{74} cage including $Ba@C_{74}$,[24] $Sm@C_{74}$,[25] $U@D_{3h}$-C_{74},[26] and $Sc_2C_2@D_{3h}(14246)$-C_{74}.[27] However, computations have suggested that for $M_2@C_{74}$, two isomers, $M_2@C_2(13295)$-C_{74} and $M_2@C_2(13333)$-C_{74}, which deviate from

Received: December 2, 2022
Published: March 20, 2023

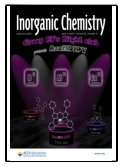

https://doi.org/10.1021/acs.inorgchem.2c04250
Inorg. Chem. 2023, 62, 5114−5122

the IPR by having two adjacent pairs of pentagons, are more stable than the $M_2@D_{3h}$-C_{74} isomer.[28] Similar predictions have been made for $Sc_2S@C_{74}$.[29] Subsequently, two endohedral fullerenes utilizing the $C_2(13333)$-C_{74} cage have been isolated and structurally characterized: $Ho_2O@C_2(13333)$-C_{74}[30] and $Dy_2O@C_2(13333)$-C_{74}.[31]

RESULTS AND DISCUSSION

Preparation and Isolation of $Tb_2O@C_2(13333)$-C_{74}. A sample of $Tb_2O@C_2(13333)$-C_{74} was obtained as a byproduct from the earlier preparation of the azafullerene $Tb_2@C_{79}N$.[13] Carbon soot containing $Tb_2O@C_2(13333)$-C_{74} was synthesized by the three-phase electric arc discharge evaporation of graphite rods doped with Tb_4O_7 powder under an atmosphere of dinitrogen.[32] The soot was subjected to a chemical separation using amino-functionalized silica,[33] followed by several rounds of HPLC on different columns as outlined in the Experimental Section. Figure 1 shows the HPLC trace of the purified material along with the experimental and computed mass spectra.

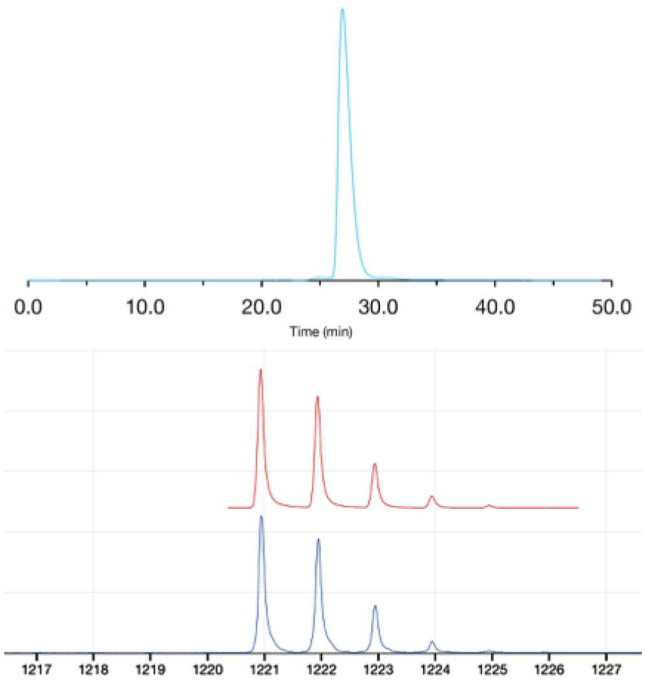

Figure 1. Top: HPLC trace of purified $Tb_2O@C_{74}$. Bottom: mass spectrum of isolated $Tb_2O@C_{74}$. Experimental spectrum $Tb_2O@C_{74}$ (lower; blue) and simulated $Tb_2O@C_{74}$ spectrum (above; red).

Figure 2 shows the UV/Vis spectrum of a sample of $Tb_2O@C_2(13333)$-C_{74} in toluene solution. The UV/Vis spectra of endohedral fullerenes are characteristic of the cage size and isomeric cage structure. Thus, the spectrum of $Tb_2O@C_2(13333)$-C_{74} with absorption maxima at 356, 406, 537, 605, 660, and a shoulder at 712 nm is similar to those of $Ho_2O@C_2(13333)$-C_{74} (with maxima at 417, 541, 612, 659, and a shoulder at 712 nm)[30] and $Dy_2O@C_2(13333)$-C_{74} (with maxima at 370, 420, 540, 610, 660, and a shoulder at 720 nm).[31] In addition, both $Ho_2O@C_2(13333)$-C_{74} and $Dy_2O@C_2(13333)$-C_{74} exhibited features in the near-IR region that we could not detect in $Tb_2O@C_2(13333)$-C_{74} due to our instrument limitations. The similarity of the UV/Vis spectra of $Ho_2O@C_2(13333)$-C_{74}, $Dy_2O@C_2(13333)$-C_{74}, and

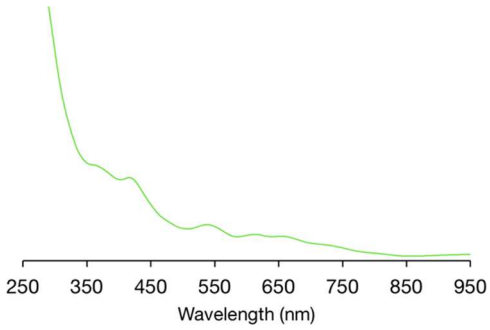

Figure 2. UV/vis spectrum of $Tb_2O@C_2(13333)$-C_{74} in toluene solution at room temperature.

$Tb_2O@C_2(13333)$-C_{74} suggests that all have the same electronic distribution: $2M^{3+}$, O^{2-}, $C_2(13333)$-C_{74}^{4-}.

Crystallographic Characterization of $Tb_2O@C_2(13333)$-C_{74}. To obtain the ordered crystal of the endohedral fullerene suitable for single-crystal X-ray diffraction, we utilized the procedure in which the endohedral is cocrystallized with $Ni^{II}(OEP)$ (OEP is the dianion of octaethylporphyrin).[34−36] Black needles of $Tb_2O@C_2(13333)$-C_{74}·$Ni(OEP)$·$1.5C_7H_8$ were obtained by diffusion of a toluene solution of $Ni^{II}(OEP)$ into a toluene solution of $Tb_2O@C_2(13333)$-C_{74} and used for the collection of X-ray diffraction data. The crystallographic data indicate that this endohedral fullerene uses a carbon cage with C_2 symmetry: $C_2(13333)$-C_{74}. Figure 3 shows how the endohedral fullerene,

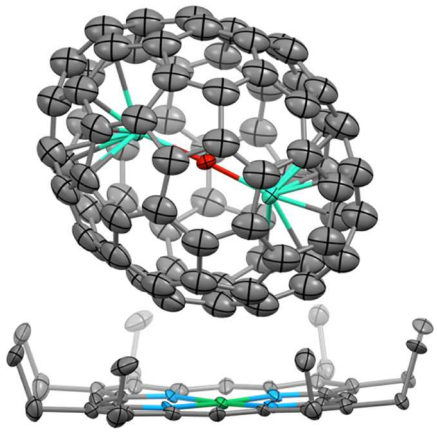

Figure 3. Relative orientation of the fullerene and metalloporphyrin in $Tb_2O@C_2(13333)$-C_{74}·$Ni^{II}(OEP)$·$1.5C_7H_8$ showing 30% thermal contours. For clarity, the toluene molecules and hydrogen atoms have been omitted. Color code: carbon, gray; oxygen, red; nitrogen, blue; nickel, green; terbium, blue-green.

$Tb_2O@C_2(13333)$-C_{74}, is cupped by the adjacent $Ni^{II}(OEP)$ molecule. As with other oblong fullerenes like C_{70},[37] the long direction of the carbon cage is canted at an angle to the porphyrin plane. Figure 4 shows a drawing of the endohedral fullerene itself, which contains two sites within the cage where two pentagons share a common edge and are highlighted in red. Thus, this cage does not obey the isolated pentagon rule (IPR), which requires that each pentagon in a fullerene cage be surrounded by five hexagons.

In crystalline $Tb_2O@C_2(13333)$-C_{74}·$Ni^{II}(OEP)$·$1.5C_7H_8$, the asymmetric unit consists of one half of the porphyrin with the other half generated by a crystallographic mirror

https://doi.org/10.1021/acs.inorgchem.2c04250
Inorg. Chem. 2023, 62, 5114−5122

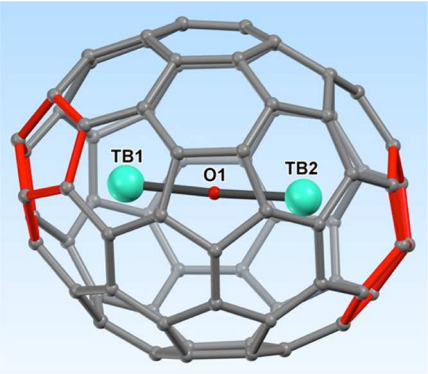

Figure 4. Structure of $Tb_2O@C_2(13333)$-C_{74} in $Tb_2O@C_2(13333)$-C_{74}·Ni^{II}(OEP)·1.5C_7H_8. Only the endohedral fullerene is shown, and the pairs of pentagons that share a common edge are highlighted in red.

plane, an entire molecule of $Tb_2O@C_2(13333)$-C_{74} at half occupancy and two sites for toluene molecules, one of which is disordered. The crystallographic mirror plane that bisects the Ni^{II}(OEP) molecule also passes through the chiral $Tb_2O@C_2(13333)$ molecule and generates the mirror image of this endohedral fullerene. Thus, the crystal is a racemate and the presence of the two enantiomers in the crystal reflects the fact that no effort was made to separate these enantiomers.

Figure 5 shows the $Tb_2O@C_2(13333)$-C_{74} molecule from a perspective that places one of the pentalene units formed by

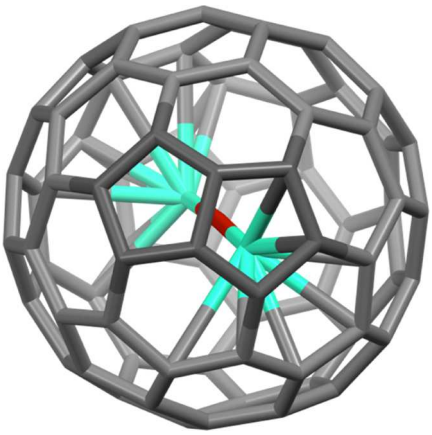

Figure 5. Structure of $Tb_2O@C_2(13333)$-C_{74} in $Tb_2O@C_2(13333)$-C_{74}·Ni^{II}(OEP)·1.5C_7H_8 showing the interaction of terbium atom with one of the pentalene units (highlighted in dark gray) formed by the junctions of two pentagons. Only the endohedral fullerene is shown. Color code: carbon, gray; oxygen, red; terbium, blue-green.

the junction of two pentagons nearest the viewer. Notice that the terbium atom nearest the pentalene unit is not situated directly over the C−C bond at the center of the pentalene unit. Instead, the terbium atom is situated to the side of the pentalene unit and makes the closest contact with some of the carbon atoms in the pentalene unit and some carbon atoms in an adjoining hexagon of the cage. A similar situation occurs at the other pentalene site, where again the terbium atom does not sit over the center C−C bond of the pentalene unit but sits to one side of that unit. In many endohedral fullerenes that contain a pentalene unit, metal atoms are centered over the central C−C bond of that unit as is the case in the following crystallographically characterized endohedrals: $Sc_3N@D_3(6275)$-C_{68},[38] $M_3N@C_s(51365)$-C_{84}, (M = Tb, Tm, or Gd),[39,40] $Gd_3N@C_s(39663)$-C_{82},[41] $M_3N@C_2(22010)$-C_{78} (M = Gd, Tb, or Ho),[42,43] $Sc_2O@C_2(7892)$-C_{70},[44] $Sm@C_{2v}(19138)$-C_{76},[45] $U@C_1(17418)$-C_{76},[46] $U@C_1(28324)$-C_{80},[13] $Th@C_1(28324)$-C_{80},[13] $Sc_2S@C_s(10528)$-C_{72},[47] $Gd_2C_2@C_1(51383)$-C_{84},[48] and $MNC@C_{2v}(19138)$-C_{76} (M = Tb, Y).[49] However, in $La_2@C_s(17490)$-C_{76}, it appears that the two lanthanum atoms are not strongly bonded to the two pentalene units but rather are situated closer to a hexagon and are able to move about the cage.[50] Additionally, the presence of cage disorder and multiple metal ion sites in the monometallic endohedral fullerenes, $U@C_1(17418)$-C_{76}, $U@C_1(28324)$-C_{80}, and $Th@C_1(28324)$-C_{80},[13] suggests that the metal-pentalene bonding in these fullerenes may not be strong.

The structure of $Tb_2O@C_2(13333)$-C_{74} is similar to the structures of $Ho_2O@C_2(13333)$-C_{74}[30] and $Dy_2O@C_2(13333)$-C_{74}.[31] All involve the non-IPR cage, $C_2(13333)$-C_{74}, and contain nearly linear M−O−M units. In $Tb_2O@C_2(13333)$-C_{74}, the Tb−O distances are identical within esd's, 2.017(9) and 2.018(9) Å, and the Tb1−O−Tb2 angle, 177.0(4), is nearly linear. The Tb−O distances are remarkably short. A survey of the Cambridge Crystallographic Data Base reveals that Tb−O distances range from 2.28 to 2.49 Å, with an average length of 2.40 Å.[51] In $Ho_2O@C_2(13333)$-C_{74}, the Ho−O bond lengths in the two crystallographically different clusters are shorter than the corresponding Tb−O distances: 2.026(5) and 1.999(5) Å in the major site and 2.001(5) and 2.008(5) Å in the minor site. The Ho−O−Ho angle is 170.5(2)° in the major site and 171.0(2)° in the minor site. For $Dy_2O@C_2(13333)$-C_{74}, disorder obscure matters but the representative Dy−O distances are reported as 1.980(5) and 2.059(5) Å and the Dy−O−Dy angle was given as 171.9(3)°. In all three of these endohedrals involving the $C_2(13333)$-C_{74} cage, the metal atoms have similar positions that are situated to the side of the pentalene unit so that the metal atoms are not positioned over that unit as frequently seen in other endohedrals as noted above.

Structural information for other endohedral fullerenes of the type $M_2O@C_{2n}$ that have been crystallographically characterized is summarized in Table 1. As the data in this table show, the M−O−M angles in these endohedral fullerenes are quite variable, but nearly linear arrangements are uncommon. A similar situation concerning M−O−M angles also exists in coordination complexes as well.[52] For example, the Fe^{III}−O−Fe^{III} bond angles in complexes containing the N_4Fe−O−FeN_4 core range from 145° to 180°.[52] Additionally, in many of the $M_2O@C_{2n}$ type endohedrals, there is a considerable disorder in the positioning of the metal atoms. In Table 1, data are shown only for the major orientation of the M_2O unit when there is a disorder in the metal atom positions. The linear nature of the M−O−M units in $M_2O@C_2(13333)$-C_{74} (M = Tb, Ho, or Dy) is likely to be related to the elongated nature of the carbon cage with the two pentalene units at opposite ends.

Computational Studies of Magnetic Properties. This study did not yield a sufficient quantity of $Tb_2O@C_2(13333)$-C_{74} to allow us to obtain experimental magnetic data. However, we investigate the magnetic properties of the $Tb_2O@C_2(13333)$-C_{74} molecule starting from the experimental geometry (i.e., atomic coordinates are in Table S1), using ab-initio multiconfigurational methods (see Supporting Information for details of the methods). Each Tb^{3+} has $4f^8$ valence electrons. According to the Hund's rules, this leads to a spin angular momentum S = 3, an orbital angular momentum

https://doi.org/10.1021/acs.inorgchem.2c04250
Inorg. Chem. 2023, 62, 5114−5122

Table 1. Structural Parameters for Crystallographically Characterized Endohedral Fullerenes Containing M_2O Units

compound	M−O−M angle (degree)	M−O distance (Å)	M−O distance (Å)	refs
$Tb_2O@C_2(13333)$-C_{74}	177.0(4)	2.017(9)	2.018(9)	a
$Ho_2O@C_2(13333)$-C_{74}	170.5(2)	2.026(5)	1.999(5)	b
$Dy_2O@C_2(13333)$-C_{74}	171.9(3)	1.980(5)	2.059(5)	c
$Ho_2O@D_{2d}(51591)$-C_{84}	176.06	1.942(6)−2.081(6)		d
$Ho_2O@D_3(85)$-C_{92}	157.3(6)	2.562(13)	2.407(11)	e
$Dy_2O@C_s(6)$-C_{82}	not determined	1.985(11) average		f
$Dy_2O@C_{3v}(8)$-C_{82}	not determined	1.978(9) average		f
$Dy_2O@C_{2v}(9)$-C_{82}.	not determined	1.944(8) average		f
$Sc_2O@C_2(7892)$-C_{70}	131.24	1.909(5)	1.909(5)	g
$Sc_2O@T_d(19151)$-C_{76}	133.9(4)	1.972(4)	1.825(5)	h
$Sc_2O@C_{2v}(3)$-C_{78}	134.38(14)	1.868(4)	1.905(4)	i
$Sc_2O@D_{3h}(5)$-C_{78}	135.21(12)	1.903(4)	1.979(4)	i
$Sc_2O@C_{2v}(5)$-C_{80}	160.79(18)	2.017(4)	1.861(4)	j
$Sc_2O@C_s(6)$-C_{82}	156.6°	1.943	1.867	k
$Sc_2O@C_{3v}(8)$-C_{82}	131.0−148.9	1.937 Å	1.888	l
$Lu_2O@C_1(31876)$-C_{80}	157.05	1.970	2.017	m
$Lu_2O@C_{2v}(5)$-C_{80}	141.80	1.914	2.083	m

[a]This paper. [b]Liu, A.; Nie, M.; Hao, Y.; Yang, Y.; Wang, T.; Slanina, Z.; Cong, H.; Feng, L.; Wang, C.; Uhlik, F., Inorg. Chem. 2019, 58, 4774−4781. [c]Velkos, G.; Yang, W.; Yao, Y.-R.; Sudarkova, S.-M.; Liu, X.-Y.; Büchner, B.; Avdoshenko, S. M.; Chen, N.; Popov, A. A., Chem. Sci. 2020, 11, 4766−4772. [d]Cong, H.; Liu, A.; Hao, Y.; Feng, L.; Slanina, Z.; Uhlik, F., Inorg. Chem. 2019, 58, 10905−10911. [e]Yu, Y.; Slanina, Z.; Wang, F.; Yang, Y.; Lian, Y.; Uhlik, F.; Xin, B.; Feng, L., Inorg. Chem. 2020, 59, 11020−11027. [f]Yang, W.; Velkos, G.; Liu, F.; Sudarkova, S. M.; Wang, Y.; Zhuang, J.; Zhang, H.; Li, X.; Zhang, X.; Büchner, B.; Avdoshenko, S. M.; Popov, A. A.; Chen, N., Adv. Sci. 2019, 6, 1901352. [g]Feng, L.; Zhang, M.; Hao, Y.; Tang, Q.; Chen, N.; Slanina, Z.; Uhlík, F., Dalton Trans. 2016, 45, 8142−8148. [h]Yang, T.; Hao, Y.; Abella, L.; Tang, Q.; Li, X.; Wan, Y.; Rodríguez-Fortea, A.; Poblet, J. M.; Feng, L.; Chen, N., Chem. - Eur. J. 2015, 21, 11110−11117. [i]Hao, Y.; Tang, Q.; Li, X.; Zhang, M.; Wan, Y.; Feng, F.; Chen, N.; Slanina, Z.; Adamowicz, L.; Uhlík, F., Inorg. Chem. 2016, 55, 11354−11361. [j]Tang, Q.; Abella, L.; Hao, Y.; Li, X.; Wan, Y.; Rodriguez-Fortea, A.; Poblet, J. M.; Feng, L.; Chen, N., Inorg. Chem. 2015, 54, 9845−9852. [k]Mercado, B. Q.: Stuart, M. A.: Mackey, M. A.; Pickens, J. E.; Confait, B. S.; Stevenson, S.; Easterling, M. L.; Valencia, R.; Rodríguez-Fortea, A.; Poblet, J. M.; Olmstead, M. M.; Balch, A. L., J. Am. Chem. *Soc.* 2010, 132, 12098−12105. [l]Tang, Q.; Abella, L.; Hao, Y.; Li, X.; Wan, Y.; Rodríguez-Fortea, A.; Poblet, J. M.: Feng, L.; Chen, N., Inorg. Chem. 2016, 55, 1926−1933. [m]Yu, P.; Li, M.; Shen, W.; Hu, S.; Yu, P.; Tian, X.; Zhao, X.; Bao, L.; Lu, X., Inorg. Chem. Front. 2022, 9, 2264−2270.

$L = 3$, and a total electronic angular momentum $J = 6$. The O^{2-} anion does not carry unpaired electrons. The low-energy spectrum of the system can be described by the following effective Hamiltonian

$$\hat{H} = \hat{H}_{LF}^{Tb1} + \hat{H}_{LF}^{Tb2} + \hat{H}_{int} \quad (1)$$

Here, the first two terms correspond to the ligand-field Hamiltonian (single-ion magnetic anisotropy) for the two Tb ions, while the third is the interaction Hamiltonian between the two Tb ions. The ligand-field Hamiltonian for ion A is given by

$$\hat{H}_{LF}^{A} = \sum_{k=2,4,6} \sum_{q=-k}^{k} B_k^q \hat{O}_q^k(\hat{J}_A) \quad (2)$$

where $\hat{O}_q^k(\hat{J}_A)$ are extended Stevens operators[53] and B_k^q are the corresponding crystal-field parameters. Here, $\hat{J}_A$ is the total angular momentum operator for the A ion. To determine the crystal-field parameters, for each Tb^{3+} ion, we replace the other Tb^{3+} ion with a nonmagnetic La^{3+}. We then calculate the low-energy spectrum using the state-average complete active space self-consistent field (SA-CASSCF) method combined with the restricted active space state interaction (RASSI) approach for the inclusion of the spin−orbit interaction (see Supporting Information for details). The spin-free energies and spin−orbit energies for $Tb_2O@C_2(13333)$-C_{74} molecules with one of the Tb^{3+} ions being replaced by a nonmagnetic La^{3+} ion are shown in Tables S2 and S3. The calculated energy levels corresponding to the ground ($J = 6$) multiplet for one of the Tb ions are shown in Figure 6. The spectrum consists of quasi-doublets (except the highest level). The tunnel splitting is small for the low-lying doublets, but it increases significantly at higher energies. The energy gap between the ground and first-excited doublets is almost 300 cm^{-1}. These features indicate the strong axiality of the molecule, which makes it a good candidate for a single-molecule magnet with a large magnetic anisotropy barrier. The crystal-field parameters are then calculated using the SINGLE_ANISO methodology.[54] Table

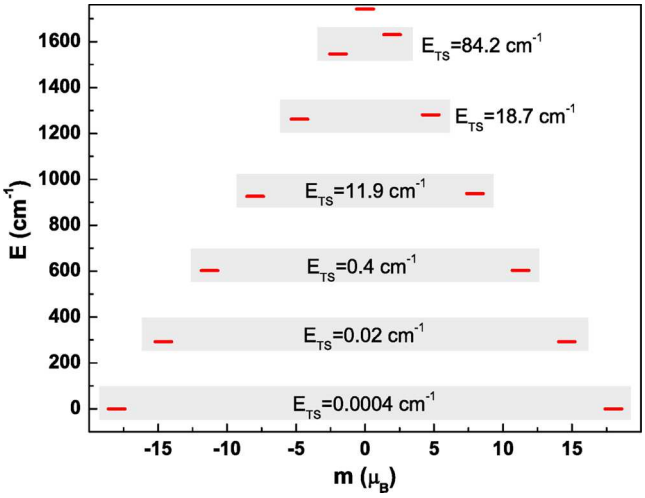

Figure 6. Ground ($J = 6$) multiplet for $Tb_2O@C_2(13333)$-C_{74} molecule with one of the Tb^{3+} ions being replaced by a nonmagnetic La^{3+} ion. The horizontal axis shows magnetic moment in units of Bohr magneton. The tunnel splitting of quasi-doublets is denoted.

https://doi.org/10.1021/acs.inorgchem.2c04250
Inorg. Chem. 2023, 62, 5114−5122

2 shows the most important crystal-field parameters calculated for one of the Tb^{3+} ion. Here, the z axis is along the Tb−O bond, which is the magnetic easy axis of the molecule. As seen, the axial parameters are much larger than the transverse parameters, confirming the strong axiality of the system. Nevertheless, the transverse parameters are non-zero and are responsible for the aforementioned tunnel splitting of the doublets. We also show the crystal-field parameters for the artificial Tb_2O molecules that were obtained from the original $Tb_2O@C_2(13333)$-C_{74} molecule by removing the fullerene cage (and again replacing one of the Tb^{3+} ion by a nonmagnetic La^{3+}). In this case, we observe much stronger axiality. This indicates that the fullerene cage enhances the transverse crystal-field interactions.

Table 2. Most Important Crystal-Field Parameters for $Tb_2O@C_2(13333)$-C_{74} and Tb_2O (No Fullerene Cage) Molecules with One of the Tb^{3+} Ions being Replaced by a Nonmagnetic La^{3+} Ion[a]

B_k^q	TbLaO@C_{74} (cm^{-1})	TbLaO (cm^{-1})
B_2^{-2}	-9.2704×10^{-1}	8.2209×10^{-4}
B_2^{-1}	-1.4998	-2.2557×10^{-2}
B_2^{0}	-1.5232×10^{1}	-1.2524×10^{1}
B_2^{1}	9.8108×10^{-1}	-1.7597×10^{-1}
B_2^{2}	-1.8203×10^{-1}	3.1539×10^{-3}
B_4^{-4}	5.0565×10^{-3}	1.4486×10^{-9}
B_4^{-3}	-2.1294×10^{-2}	1.9547×10^{-7}
B_4^{-2}	1.1303×10^{-2}	-2.1189×10^{-6}
B_4^{-1}	-3.3205×10^{-4}	1.4655×10^{-5}
B_4^{0}	2.9938×10^{-2}	2.2858×10^{-2}
B_4^{1}	-1.4818×10^{-2}	1.1434×10^{-4}
B_4^{2}	-3.0491×10^{-3}	-8.1293×10^{-6}
B_4^{3}	9.2596×10^{-3}	4.8457×10^{-7}
B_4^{4}	1.0387×10^{-2}	2.8364×10^{-9}

[a]The full set of crystal-field parameters is provided in Table S5 of the Supporting Information. Here, we use the same coordinates as the atomic coordinates shown in Table S1.

The crystal-field parameters for the second Tb^{3+} ion are shown in the Supporting Information (Table S5). While, in general, these parameters have similar features to the first Tb^{3+} ion, the transverse interactions are significantly stronger. The main reason for this is that we use the common z axis for both Tb^{3+} ions, which is the magnetic easy axis for the first Tb^{3+} ion. The magnetic easy axis of the second Tb^{3+} ion is along the O−Tb bonding direction, and it deviates from the easy axis of the first Tb^{3+} ion by around 3°. This result is consistent with the fact that the Tb−O−Tb angle is 3° short of the completely linear alignment.

The magnetic interaction Hamiltonian consists of two contributions, the exchange and dipolar interactions. To estimate the magnetic exchange interaction in the $Tb_2O@C_2(13333)$-C_{74} molecule, we first calculate the energy difference between the ferromagnetic and antiferromagnetic arrangements of the Tb spins (S_{tot} = 6 and S_{tot} = 0) in the absence of spin−orbit coupling, using the SA-CAS(16,14)SCF method (see Table S4 and SI for details). Here, S_{tot} is the total spin angular momentum of the $Tb_2O@C_2(13333)$-C_{74} molecule. The calculated energy difference, $\Delta_{FM\text{-}AFM}$, is −9.4 cm^{-1}, which indicates that the ferromagnetic arrangement has a lower energy than the antiferromagnetic arrangement. Calculations for the Tb_2O molecule show that the effect of the fullerene cage is negligible.

For a proper calculation of the exchange coupling for multi-ions with unquenched orbital angular momentum, the spin−orbit interaction needs to be included. Note that the energy difference $\Delta_{FM\text{-}AFM}$ is much smaller than the ligand-field splitting (Table S2) and the RASSI-SO energy difference between the ground and the first-excited quasi-doublets of each Tb ion in the molecule (see Table S3). Therefore, the anisotropic exchange interaction in the presence of spin−orbit interaction can be described by the Lines model[55] implemented in the POLY_ANISO program.[56−59] Although an elaborate model[60] including anisotropic and higher-order exchange coupling parameters for J multiplets was proposed for an accurate description of exchange interactions in multi-ion systems with strong spin−orbit interaction, the Lines model has been shown to successfully explain experimental data.[61−63] The ground quasi-doublet corresponds to $|m_J| = 6$ states. Thus, the ground quasi-doublet of each Tb ion can be projected onto pseudospin $s = 1/2$. The exchange interaction of the $Tb_2O@C_2(13333)$-C_{74} molecule including spin−orbit interaction can be described by the anisotropic Ising model with two pseudospins $s_{Tb1} = 1/2$ and $s_{Tb2} = 1/2$, each of which represents a Tb ion. Using the $\Delta_{FM\text{-}AFM}$ value and the SINGLE_ANISO results of the two fragments (TbLaO@C_{74} and LaTbO@C_{74}) as input for the POLY_ANISO program, we find that the ground and higher doublets are separated by 8.1 cm^{-1}. As a result, the anisotropic exchange coupling J_{ex} for the pseudospins is 16.2 cm^{-1} in the following effective Ising Hamiltonian

$$\hat{\boldsymbol{H}}_{ex} = -\boldsymbol{J}_{ex}\hat{\boldsymbol{s}}_{Tb1,z'}\hat{\boldsymbol{s}}_{Tb2,z'} \tag{3}$$

where $\hat{s}_{A,z'}$ is the z' component of the pseudospin angular momentum operator of ion A. The z' axis coincides with the direction connecting the Tb ions. The calculation details can be found in the Supporting Information.

The magnetic dipole−dipole coupling is also calculated using the POLY_ANISO program for the projected lowest-energy doublets. We find that the magnetic dipole−dipole interaction favors the ferromagnetic arrangement by 2.1 cm^{-1}. This value is very similar to our calculation of the magnetic dipole−dipole coupling, assuming that classical magnetic moments of magnitude $m = g_L J\mu_B = 9\mu_B$ reside at the Tb ion positions, where μ_B is Bohr magneton. The magnetic moment points in the direction of the easy axis of the corresponding Tb ion. The dipolar energy is given by

$$E_{dip} = \frac{-\mu_0}{4\pi r^5}(3(\boldsymbol{m}_{Tb1}\cdot\boldsymbol{r})(\boldsymbol{m}_{Tb2}\cdot\boldsymbol{r}) - \boldsymbol{m}_{Tb1}\cdot\boldsymbol{m}_{Tb2}r^2) \tag{4}$$

where $\boldsymbol{m}_{Tb1}$ and $\boldsymbol{m}_{Tb2}$ are magnetic moment vectors of the two Tb ions and $\boldsymbol{r}$ is the vector connecting the two Tb ions. Since both magnetic moments are approximately parallel to $\boldsymbol{r}$, the ferromagnetic configuration of the moments has a lower energy than the antiferromagnetic configuration. Thus, the dipolar interaction has the same sign as the exchange coupling. However, the calculated energy difference between the antiferromagnetic and ferromagnetic configurations is only 2 cm^{-1}. This is an order of magnitude lower than in the case of the exchange coupling, and therefore, the dipolar coupling has a rather small effect.

Based on the calculated energy spectrum of the magnetic interaction, we compute static molar magnetic susceptibility χ

https://doi.org/10.1021/acs.inorgchem.2c04250
Inorg. Chem. 2023, 62, 5114−5122

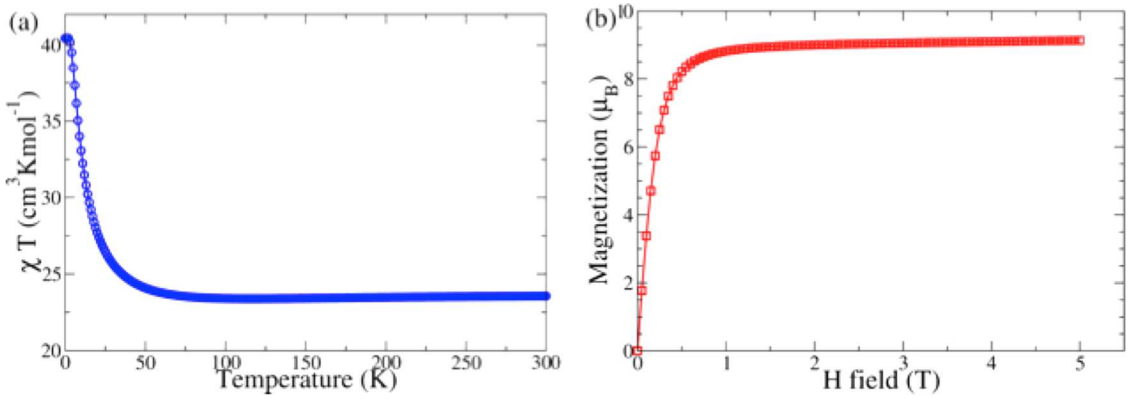

Figure 7. (a) Calculated molar magnetic susceptibility multiplied by temperature as a function of temperature, and (b) the calculated magnetization at 2 K as a function of magnetic field for the $Tb_2O@C_2(13333)$-C_{74} molecule, using the POLY_ANISO program.

as a function of temperature (T) (Figure 7a) and magnetization as a function of magnetic H field (Figure 7b). Future experiments on a crystal sample of the molecules can be compared with the calculated results.

Now, we compare the magnetic properties of $Tb_2O@C_2(13333)$-C_{74} to those of other endohedral fullerenes with similar structures such as $Ho_2O@C_2(13333)$-C_{74}[30] and $Dy_2O@C_2(13333)$-C_{74}[31] in the literature. There are additional ab-initio calculations on related endohedral fullerenes.[32,64−67] Since the magnetic interactions between the M^{3+} ions are very weak in all three compounds, the magnetic properties of the compounds are mainly governed by those of the individual M^{3+} ions. In $Tb_2O@C_2(13333)$-C_{74} and $Ho_2O@C_2(13333)$-C_{74}, the M^{3+} ions are non-Kramers systems with tunnel splitting between quasi-doublets, while in $Dy_2O@C_2(13333)$-C_{74}, the M^{3+} ions are Kramers systems with exactly degenerate doublets. Interestingly, although the crystal-field environment is similar for the three compounds, $Tb_2O@C_2(13333)$-C_{74} and $Dy_2O@C_2(13333)$-C_{74} have strongly axial crystal fields, while that is not the case for $Ho_2O@C_2(13333)$-C_{74} based on the experimental magnetization data. More specifically, the ground state of $Tb_2O@C_2(13333)$-C_{74} or $Dy_2O@C_2(13333)$-C_{74} is approximately $|m_J| = J$, whereas the ground state of $Ho_2O@C_2(13333)$-C_{74} is either $|m_J| = 4$ ($<J = 8$) or a linear combination of several different m_J values ($|m_J| < J$). This situation may be attributed to the fact that different M^{3+} ions have distinct electron density distributions and that the magnetic anisotropy is strongly correlated to the electron density of the M^{3+} ion.[68] The calculated crystal-field splitting of a single M^{3+} ion in $Dy_2O@C_2(13333)$-C_{74} is comparable to that in $Tb_2O@C_2(13333)$-C_{74}. The magnetic dipolar interaction between the two M^{3+} ions in $Dy_2O@C_2(13333)$-C_{74} also has a ferromagnetic character, and the dipolar interaction energy difference between the ferromagnetic and antiferromagnetic configurations is comparable to that in $Tb_2O@C_2(13333)$-C_{74}.

■ CONCLUSIONS

The first endohedral fullerene to contain a terbium oxide unit has been synthesized and structurally identified. $Tb_2O@C_2(13333)$ contains a nearly linear Tb−O−Tb unit housed within a non-IPR cage that contains two pairs of adjacent pentagons. In non-IPR endohedrals, the metal ions usually reside near the adjacent pentagons. However, in $Tb_2O@C_2(13333)$, the terbium ions are not centered over the pentalene units but are situated to the sides of these units. The magnetic properties of the $Tb_2O@C_2(13333)$-C_{74} molecule have been examined computationally. These studies indicate that $Tb_2O@C_2(13333)$-C_{74} should be a single-molecule magnet with strong axiality and a large magnetic anisotropy barrier.

■ EXPERIMENTAL SECTION

Synthesis and Purification of $Tb_2O@C_2(13333)$. $Tb_2O@C_{74}$ was synthesized using a three-phase electric arc discharge evaporation of graphite rods doped with Tb_4O_7 powder (Jiayuan Advanced Materials Co., Ltd.) by injection into the three-phase electric arc zone in a N_2 atmosphere.[69] An HPLC trace of the product mixture after chemical separation using amino-functionalized silica[34] is shown in Figure S1 of ref 32. The sample was then subjected to multiple collection passes with 100 μL injections with a PBB column (4.6 mm I.D. × 250 mm); λ = 390 nm; flow rate 1.0 mL min^{-1}; 1:1 1,2-dichlorobenzene/toluene as eluent to remove the $Tb_2@C_{79}N$ and $Tb_3N@C_{80}$. The remaining mixture with most of the $Tb_3N@C_{80}$ and $Tb_2@C_{79}N$ removed was then concentrated using a rotovap and injected in 500 μL portions onto a 10 mm × 250 mm PYE column using toluene as the eluent at 4 mL min^{-1}. Twenty-three separate fractions were collected. Fraction 8 (collected from 13.8 to 16.8 min) contained the $Tb_2O@C_{74}$ mixed primarily with empty-cage C_{84}. Fraction 8 was concentrated and further separated using a 4.6 mm × 250 mm PBB column with toluene as the eluent at 1.0 mL min^{-1}. The fraction collected from 30.0 to 34.5 min contained primarily $Tb_2O@C_2(13333)$. An HPLC trace of $Tb_2O@C_2(13333)$ that was collected from this fraction using a 4.6 mm × 250 mm Buckyprep column with toluene as the eluent at 1 mL min^{-1} is shown in Figure 1. A mass spectrum of $Tb_2O@C_2(13333)$ is also shown in Figure 1.

Single-Crystal X-ray Diffraction. Crystals were grown by slow diffusion of a filtered toluene solution containing nickel(II) octaethylporphyrin into a filtered toluene solution containing $Tb_2O@C_2(13333)$-C_{74}. One of the black needles that formed was mounted in the nitrogen cold stream produced by an Oxford Cryostream low-temperature device on the goniometer head of a Bruker D8 diffractometer equipped with a PHOTON 2 CMOS detector at beamline 12.2.1 of the Advanced Light Source (Lawrence Berkeley National Laboratory, Berkeley, CA). Data were collected with the use of silicon (111) monochromated synchrotron radiation (λ = 0.7288 Å). The data sets were reduced with the use of Bruker SAINT, and a multiscan absorption correction was applied with the use of SADABS or TWINABS. The structures were determined by direct methods and refined by full-matrix least-squares on F^2 (SHELXL-2018).[70,71] See Supporting Information for further refinement details.[72]

https://doi.org/10.1021/acs.inorgchem.2c04250
Inorg. Chem. 2023, 62, 5114−5122

■ ASSOCIATED CONTENT

Supporting Information

The Supporting Information is available free of charge at https://pubs.acs.org/doi/10.1021/acs.inorgchem.2c04250.

Information regarding the details of the computational studies (PDF)

Accession Codes

CCDC 2184521 contains the supplementary crystallographic data for this paper. These data can be obtained free of charge via www.ccdc.cam.ac.uk/data_request/cif, or by emailing data_request@ccdc.cam.ac.uk, or by contacting The Cambridge Crystallographic Data Centre, 12 Union Road, Cambridge CB2 1EZ, UK; fax: +44 1223 336033.

■ AUTHOR INFORMATION

Corresponding Authors

Harry C. Dorn − *Department of Chemistry, Virginia Polytechnic Institute and State University, Blacksburg, Virginia 24061, United States;* orcid.org/0000-0002-3150-5314; Email: hdorn@vt.edu

Alan L. Balch − *Department of Chemistry, University of California, Davis, Davis, California 95616, United States;* orcid.org/0000-0002-8813-6281; Email: albalch@ucdavis.edu

Authors

James C. Duchamp − *Department of Chemistry, Emory and Henry College, Emory, Virginia 24327, United States;* orcid.org/0000-0001-7619-3353

Aleksander L. Wysocki − *Department of Physics, Virginia Polytechnic Institute and State University, Blacksburg, Virginia 24061, United States*

Kyungwha Park − *Department of Physics, Virginia Polytechnic Institute and State University, Blacksburg, Virginia 24061, United States;* orcid.org/0000-0002-0597-204X

Marilyn M. Olmstead − *Department of Chemistry, University of California, Davis, Davis, California 95616, United States;* orcid.org/0000-0002-6160-1622

Mrittika Roy − *Department of Chemistry, University of California, Davis, Davis, California 95616, United States*

Complete contact information is available at: https://pubs.acs.org/10.1021/acs.inorgchem.2c04250

Notes

The authors declare no competing financial interest.

■ ACKNOWLEDGMENTS

This paper is dedicated to the memory of the late Professor Marilyn M. Olmstead. $Tb_2O@C_2(13333)$ was the last fullerene structure she was able to complete. The authors thank the National Science Foundation for financial support (Grant CHE-1807637 to A.L.B. and M.M.O.) and the Department of Energy (DOE) Basic Energy Sciences (BES) Grant DE-SC0018326 (K.P. and A.L.W.). Computational support was provided by the Virginia Tech Advanced Research Center and the Extreme Science and Engineering Discovery Environment (XSEDE) under Project number DMR060009N, which is supported by the National Science Foundation Grant number ACI-1548562. This research used resources of the Advanced Light Source, which is a DOE Office of Science User Facility under contract no. DE-AC02-05CH11231. The authors thank Dr. S.J. Teat for assistance and Kyle Kirkpatrick for help in the early stages of the project.

■ REFERENCES

(1) Rodríguez-Fortea, A.; Balch, A. L.; Poblet, J. M. Endohedral metallofullerenes: a unique host−guest association. *Chem. Soc. Rev.* **2011**, *40*, 3551−3563.

(2) Lu, X.; Feng, L.; Akasaka, T.; Nagase, S. Current status and future developments of endohedral metallofullerenes. *Chem. Soc. Rev.* **2012**, *41*, 7723−7760.

(3) Cong, H. L.; Yu, B.; Akasaka, T.; Lu, X. Endohedral metallofullerenes: An unconventional core−shell coordination union. *Coord. Chem. Rev* **2013**, *257*, 2880−2898.

(4) Popov, A. A.; Yang, S.; Dunsch, L. Endohedral Fullerenes. *Chem. Rev.* **2013**, *113*, 5989−6113.

(5) *Endohedral Metallofullerenes: Basics and Applications*; Lu, X.; Echegoyen, L.; Balch, A. L.; Nagase, S.; Akasaka, T., Eds.; CRC Press: Boca Raton, 2014.

(6) Mikawa, M.; Kato, H.; Okumura, M.; Narazaki, M.; Kanazawa, Y.; Miwa, N.; Shinohara, H. Paramagnetic water-soluble metallofullerenes having the highest relaxivity for MRI contrast agents. *Bioconjugate Chem.* **2001**, *12*, 510−514.

(7) Ghiassi, K. B.; Olmstead, M. M.; Balch, A. L. Gadolinium-containing endohedral fullerenes: structures and function as magnetic resonance imaging (MRI) agents. *Dalton Trans.* **2014**, *43*, 7346−7358.

(8) Li, T.; Dorn, H. C. Biomedical Applications of Metal-Encapsulated Fullerene Nanoparticles. *Small* **2017**, *13*, No. 1603152.

(9) Iezzi, E. B.; Duchamp, J. C.; Fletcher, K. R.; Glass, T. E.; Dorn, H. C. Lutetium-Based Trimetallic Nitride Endohedral Metallofullerenes: New Contrast Agents. *Nano Lett.* **2002**, *2*, 1187−1190.

(10) Shultz, M. D.; Duchamp, J. C.; Wilson, J. D.; Shu, C.-Y.; Ge, J.; Zhang, J.; Gibson, H. W.; Fillmore, H. L.; Hirsch, J. I.; Dorn, H. C.; Fatouros, P. P. Encapsulation of a Radiolabeled Cluster Inside a Fullerene Cage, $^{177}Lu_xLu_{(3-x)}N@C_{80}$: An Interleukin-13-Conjugated Radiolabeled Metallofullerene Platform. *J. Am. Chem. Soc.* **2010**, *132*, 4980−4981.

(11) Liu, F.; Krylov, D. S.; Spree, L.; Avdoshenko, S. M.; Samoylova, N. A.; Rosenkranz, M.; Kostanyan, A.; Greber, T.; Wolter, A. U. B.; Büchner, B.; Popov, A. A. Single molecule magnet with an unpaired electron trapped between two lanthanide ions inside a fullerene. *Nat. Commun.* **2017**, *8*, No. 16098.

(12) Schlesier, C.; Spree, L.; Kostanyan, A.; Westerstrom, R.; Brandenburg, A.; Wolter, A. U. B.; Yang, S.-F.; Greber, T.; Popov, A. A. Strong carbon cage influence on the single molecule magnetism in Dy−Sc nitride clusterfullerenes. *Chem. Commun.* **2018**, *54*, 9730−9733.

(13) Velkos, G.; Krylov, D. S.; Kirkpatrick, K.; Spree, L.; Dubrovin, V.; Büchner, B.; Avdoshenko, S. M.; Bezmelnitsyn, V.; Davis, S.; Faust, P.; Duchamp, J.; Dorn, H. C.; Popov, A. A. High Blocking Temperature of Magnetization and Giant Coercivity in the Azafullerene $Tb_2@C_{79}N$ with a Single-Electron Terbium−Terbium Bond. *Angew. Chem., Int. Ed.* **2019**, *58*, 5891−5896.

(14) Stevenson, S.; Mackey, M. A.; Stuart, M. A.; Philips, J. P.; Easterling, M. L.; Chancellor, C. J.; Olmstead, M. M.; Balch, A. L. A Distorted Tetrahedral Metal Oxide Cluster inside an Icosahedral Carbon Cage, Synthesis, Isolation, and Structural Characterization of $Sc_4(\mu_3\text{-}O)_2@I_h\text{-}C_{80}$. *J. Am. Chem. Soc.* **2008**, *130*, 11844−11845.

(15) Feng, L.; Hao, Y.; Liu, A.; Slanina, Z. Trapping Metallic Oxide Clusters inside Fullerene Cages. *Acc. Chem. Res.* **2019**, *52*, 1802−1811.

(16) Abella, L.; Wang, Y.; Rodríguez-Fortea, A.; Chen, N.; Poblet, J. M. Current status of oxide clusterfullerenes. *Inorg. Chim. Acta* **2017**, *468*, 91−104.

(17) Mercado, B. Q.; Olmstead, M. M.; Beavers, C. M.; Easterling, M. L.; Stevenson, S.; Mackey, M. A.; Coumbe, C. E.; Phillips, J. D.; Phillips, J. P.; Poblet, J. M.; Balch, A. L. A seven atom cluster in a carbon cage, the crystallographically determined structure of $Sc_4(\mu_3\text{-}O)_3@I_h\text{-}C_{80}$. *Chem. Commun.* **2010**, *46*, 279−281.

(18) Abella, L.; Tang, Q.; Zhang, X.; Wang, Y.; Chen, N.; Poblet, J. M.; Rodríguez-Fortea, A. $Sc_3O@I_h(7)$-C_{80}: A Trimetallic Oxide Clusterfullerene Abundant in the Raw Soot. *J. Phys. Chem. C* **2016**, *120*, 26159−26167.
(19) Mercado, B. Q.; Stuart, M. A.; Mackey, M. A.; Pickens, J. E.; Confait, B. S.; Stevenson, S.; Easterling, M. L.; Valencia, R.; Rodríguez-Fortea, A.; Poblet, J. M.; Olmstead, M. M.; Balch, A. L. $Sc_2(\mu_2\text{-O})$ Trapped in a Fullerene Cage: The Isolation and Structural Characterization of $Sc_2(\mu_2\text{-O})@C_s(6)$-$C_{82}$ and the Relevance of the Thermal and Entropic Effects in Fullerene Isomer Selection. *J. Am. Chem. Soc.* **2010**, *132*, 12098−12105.
(20) Diener, M. D.; Alford, J. M. Isolation and properties of small-bandgap fullerenes. *Nature* **1998**, *393*, 668−671.
(21) Yeretzian, C.; Wiley, J. B.; Holczer, K.; Su, T.; Nguyen, S.; Kaner, R. B.; Whetten, R. L. Partial Separation of Fullerenes by Gradient Sublimation. *J. Phys. Chem. A* **1993**, *97*, 10097−10101.
(22) Goryunkov, A. A.; Markov, V. Y.; Ioffe, I. N.; Bolskar, R. D.; Diener, M. D.; Kuvychko, I. V.; Strauss, S. H.; Boltalina, O. V. $C_{74}F_{38}$: An Exohedral Derivative of a Small-Bandgap Fullerene with D_3 Symmetry. *Angew. Chem., Int. Ed.* **2004**, *43*, 997.
(23) Shustova, N. B.; Newell, B. S.; Miller, S. M.; Anderson, O. P.; Bolskar, R. D.; Seppelt, K.; Popov, A. A.; Boltalina, O. V.; Strauss, S. H. Discovering and Verifying Elusive Fullerene Cage Isomers: Structures of C_2-p^{11}-$(C_{74}$-$D_{3h})(CF_3)_{12}$ and C_2-p^{11}-$(C_{78}$-$D_{3h}(5))$-$(CF_3)_{12}$. *Angew. Chem.* **2007**, *119*, 4189−4192.
(24) Reich, A.; Panthöfer, M.; Modrow, H.; Wedig, U.; Jansen, M. The Structure of $Ba@C_{74}$. *J. Am. Chem. Soc.* **2004**, *126*, 14428−14434.
(25) Xu, W.; Hao, Y.; Uhlik, F.; Shi, Z.; Slanina, Z.; Feng, L. Structural and electrochemical studies of $Sm@D_{3h}$-C_{74} reveal a weak metal−cage interaction and a small band gap species. *Nanoscale* **2013**, *5*, 10409−10413.
(26) Cai, W.; Morales-Martinez, R.; Zhang, X.; Najera, D.; Romero, E. L.; Metta-Magaña, A.; Rodriguez-Fortea, A.; Fortier, S.; Chen, N.; Poblet, J. M.; Echegoyen, L. Single crystal structures and theoretical calculations of uranium endohedral metallofullerenes ($U@C_{2n}$, $2n$ = 74, 82) show cage isomer dependent oxidation states for U. *Chem. Sci.* **2017**, *8*, 5282−5290.
(27) Wang, Y.; Tang, Q.; Feng, L.; Chen, N. A Missing Piece of the Clusterfullerene Puzzle. *Inorg. Chem.* **2017**, *56*, 1974−1980.
(28) Zheng, H.; Zhao, X.; Ren, T.; Wang, W.-W. C_{74} endohedral metallofullerenes violating the isolated pentagon rule: a density functional theory study. *Nanoscale* **2012**, *4*, 4530−4536.
(29) Gan, L.-H.; Chang, Q.; Zhao, C.; Wang, C.-R. $Sc_2S@C_{74}$ Linear Metal Sulfide Cluster inside an IPR−violating Fullerene. *Chem. Phys. Lett.* **2013**, *570*, 121−124.
(30) Liu, A.; Nie, M.; Hao, Y.; Yang, Y.; Wang, T.; Slanina, Z.; Cong, H.; Feng, L.; Wang, C.; Uhlik, F. $Ho_2O@C_{74}$: Ho_2O Cluster Expands within a Small Non-IPR Fullerene Cage of $C_2(13333)$-C_{74}. *Inorg. Chem.* **2019**, *58*, 4774−4781.
(31) Velkos, G.; Yang, W.; Yao, Y.-R.; Sudarkova, S-M.; Liu, X.-Y.; Büchner, B.; Avdoshenko, S. M.; Chen, N.; Popov, A. A. Shape-adaptive single-molecule magnetism and hysteresis up to 14 K in oxide clusterfullerenes $Dy_2O@C_{72}$ and $Dy_2O@C_{74}$ with fused pentagon pairs and flexible Dy−$(\mu_2$-O)−Dy angle. *Chem. Sci.* **2020**, *11*, 4766−4772.
(32) Bezmelnitsyn, V.; Davis, S.; Zhou, Z. Efficient Synthesis of Endohedral Metallofullerenes in 3-Phase Arc Discharge. *Fullerenes, Nanotubes, Carbon Nanostruct.* **2015**, *23*, 612−617.
(33) Stevenson, S.; Harich, K.; Yu, H.; Stephen, R. R.; Heaps, D.; Coumbe, C.; Phillips, J. P. Nonchromatographic "Stir and Filter Approach" (SAFA) for Isolating $Sc_3N@C_{80}$ Metallofullerenes. *J. Am. Chem. Soc.* **2006**, *128*, 8829−8835.
(34) Olmstead, M. M.; Costa, D. A.; Maitra, K.; Noll, B. C.; Phillips, S. L.; Van Calcar, P. M.; Balch, A. L. Interaction of Curved and Flat Molecular Surfaces. The Structures of Crystalline Compounds Composed of Fullerene (C_{60}, $C_{60}O$, C_{70}, and $C_{120}O$) and Metal Octaethylporphyrin Units. *J. Am. Chem. Soc.* **1999**, *121*, 7090−7097.
(35) Stevenson, S.; Rice, G.; Glass, T.; Harich, K.; Cromer, F.; Jordan, M. R.; Craft, J.; Hadju, E.; Bible, R.; Olmstead, M. M.; Maitra, K.; Fisher, A. J.; Balch, A. L.; Dorn, H. C. Small-bandgap endohedral metallofullerenes in high yield and purity. *Nature* **1999**, *401*, 55−57.
(36) Roy, M.; Olmstead, M. M.; Balch, A. L. Metal Ion Effects on Fullerene/Porphyrin Cocrystallization. *Cryst. Growth Des.* **2019**, *19*, 6743−6751.
(37) Baldauf, L. M.; Ghiassi, K. B.; Olmstead, M. M.; Balch, A. L. Fullerene nanostructures: how the oblong shape of C_{70} forms a cocrystal with an enormous asymmetric unit and related cocrystals. *Nanoscale* **2020**, *12*, 20356−20363.
(38) Olmstead, M. M.; Lee, H. M.; Duchamp, J. C.; Stevenson, S.; Marciu, D.; Dorn, H. C.; Balch, A. L. $Sc_3N@C_{68}$: Folded Pentalene Coordination in an Endohedral Fullerene that Does Not Obey the Isolated Pentagon Rule. *Angew. Chem.* **2003**, *115*, 928−931.
(39) Beavers, C. M.; Zuo, T.; Duchamp, J. C.; Harich, K.; Dorn, H. C.; Olmstead, M. M.; Balch, A. L. $Tb_3N@C_{84}$: An Improbable, Egg-shaped Endohedral Fullerene that Violates the Isolated Pentagon Rule. *J. Am. Chem. Soc.* **2006**, *128*, 11352−11353.
(40) Zuo, T.; Walker, K.; Olmstead, M. M.; Melin, F.; Holloway, B. C.; Echegoyen, L.; Dorn, H. C.; Chaur, M. N.; Chancellor, C. J.; Beavers, C. M.; Balch, A. L.; Athans, A. J. New egg-shaped fullerenes: non-isolated pentagon structure of $Tm_3N@C_s(51365)$-C_{84} and $Gd_3N@C_s(51365)$-C_{84}. *Chem. Commun.* **2008**, 1067−1069.
(41) Mercado, B. Q.; Beavers, C. M.; Olmstead, M. M.; Chaur, M. N.; Walker, K.; Holloway, B. C.; Echegoyen, L.; Balch, A. L. Is the Isolated Pentagon Rule Merely a Suggestion for Endohedral Fullerenes? The structure of a Second Egg-Shaped Endohedral Fullerene − $Gd_3N@C_s(39663)$−C_{82}. *J. Am. Chem. Soc.* **2008**, *130*, 7854−7855.
(42) Beavers, C. M.; Chaur, M. N.; Olmstead, M. M.; Echegoyen, L.; Balch, A. L. Large Metal Ions in a Relatively Small Fullerene Cage: The Structure of $Gd_3N@C_2(22010)$-C_{78} Departs from the Isolated Pentagon Rule. *J. Am. Chem. Soc.* **2009**, *131*, 11519−11524.
(43) Stevenson, S.; Rothgeb, A. J.; Tepper, K. R.; Duchamp, J.; Dorn, H. C.; Powers, X. B.; Roy, M.; Olmstead, M. M.; Balch, A. L. Isolation and Crystallographic Characterization of Two, Nonisolated Pentagon Endohedral Fullerenes: $Ho_3N@C_2(22010)$-C_{78} and $Tb_3N@C_2(22010)$-C_{78}. *Chem. - Eur. J.* **2019**, *25*, 12545−12551.
(44) Feng, L.; Zhang, M.; Hao, Y.; Tang, Q.; Chen, N.; Slanina, Z.; Uhlík, F. Endohedrally stabilized C_{70} isomer with fused pentagons characterized by crystallography. *Dalton Trans.* **2016**, *45*, 8142−8148.
(45) Hao, Y. J.; Feng, L.; Xu, W.; Gu, Z. G.; Hu, Z. Q.; Shi, Z. J.; Slanina, Z.; Uhlik, F. $Sm@C_{2v}(19138)$-C_{76}: A Non-IPR Cage Stabilized by a Divalent Metal Ion. *Inorg. Chem.* **2015**, *54*, 4243−4248.
(46) Cai, W. T.; Abella, L.; Zhuang, J. X.; Zhang, X. X.; Feng, L.; Wang, Y. F.; Martinez, R. M.; Esper, R.; Boero, M.; Magana, A. M.; Fortea, A. R.; Poblet, J. M.; Echegoyen, L.; Chen, N. Synthesis and Characterization of Non-Isolated-Pentagon-Rule Actinide Endohedral Metallofullerenes $U@C_1(17418)$-C_{76}, $U@C_1(28324)$-C_{80}, and $Th@C_1(28324)$-C_{80}: Low-Symmetry Cage Selection Directed by a Tetravalent Ion. *J. Am. Chem. Soc.* **2018**, *140*, 18039−18050.
(47) Chen, N.; Beavers, C. M.; Gas, M. M.; Fortea, A. R.; Munoz, E. J.; Li, Y. Y.; Olmstead, M. M.; Balch, A. L.; Poblet, J. M.; Echegoyen, L. $Sc_2S@C_s(10528)$-C_{72}: A Dimetallic Sulfide Endohedral Fullerene with a Non Isolated Pentagon Rule Cage. *J. Am. Chem. Soc.* **2012**, *134*, 7851−7860.
(48) Zhang, J. Y.; Bowles, F. L.; Bearden, D. W.; Ray, W. K.; Ye, T.; Fuhrer, Y. Q.; Dixon, C.; Harich, K.; Helm, R. F.; Olmstead, M. M.; Balch, A. L.; Dorn, H. C. A missing link in the transformation from asymmetric to symmetric metallofullerene cages implies a top-down fullerene formation mechanism. *Nat. Chem.* **2013**, *5*, 880−885.
(49) Liu, F. P.; Wang, S.; Gao, C. L.; Deng, Q. M.; Zhu, X. J.; Kostanyan, A.; Westerström, R.; Jin, F.; Xie, S. Y.; Popov, A. A.; Greber, T.; Yang, S. F. Mononuclear Clusterfullerene Single-Molecule Magnet Containing Strained Fused-Pentagons Stabilized by a Nearly Linear Metal Cyanide Cluster. *Angew. Chem.* **2017**, *129*, 1856−1860.

https://doi.org/10.1021/acs.inorgchem.2c04250
Inorg. Chem. 2023, 62, 5114−5122

(50) Suzuki, M.; Mizorogi, N.; Yang, T.; Uhlik, F.; Slanina, Z.; Zhao, X.; Yamada, M.; Maeda, Y.; Hasegawa, T.; Nagase, S.; Lu, X.; Akasaka, T. $La_2@C_s(17\ 490)$-C_{76}: A New Non-IPR Dimetallic Metallofullerene Featuring Unexpectedly Weak Metal−Pentalene Interactions. *Chem. - Eur. J.* **2013**, *19*, 17125−17130.
(51) Groom, C. R.; Bruno, I. J.; Lightfoot, M. P.; Ward, S. C. The Cambridge Structural Database. *Acta Crystallogr., Sect. B: Struct. Sci., Cryst. Eng. Mater.* **2016**, *72*, 171−179.
(52) Lee, H. M.; Olmstead, M. M.; Gross, G. G.; Balch, A. L. Cocrystallization of Binuclear Iron(III) Porphyrins with C_{60}: Bending of μ-O{Fe^{III}(Octaethylporphyrin)} and the First Structure of the Iron(III) Octaethyloxophlorin Dimer. *Cryst. Growth Des.* **2003**, *3*, 691−697.
(53) Rudowicz, C. Transformation relations for the conventional O_k^q and normalised O'^q_k Stevens operator equivalents with k=1 to 6 and -k⩽q⩽k. *J. Phys. C: Solid State Phys.* **1985**, *18*, 1415−1430.
(54) Chibotaru, L. F.; Ungur, L. *Ab initio* calculation of anisotropic magnetic properties of complexes. I. Unique definition of pseudospin Hamiltonians and their derivation. *J. Chem. Phys.* **2012**, *137*, No. 064112.
(55) Lines, M. E. Orbital angular momentum in the theory of paramagnetic clusters. *J. Chem. Phys.* **1971**, *55*, 2977−2984.
(56) Chibotaru, L. F.; Ungur, L. *The Computer Programs SINGLE_ANISO and POLY_ANISO*; University of Leuven, 2006.
(57) Chibotaru, L. F.; Ungur, L.; Soncini, A. Origin of non-magnetic Kramers doublets in the ground state of dysprosium triangles: Evidence for toroidal magnetic moment. *Angew. Chem.* **2008**, *120*, 4194−4197.
(58) Ungur, L.; Van den Heuvel, W.; Chibotaru, L. F. Ab initio investigation of non-collinear magnetic structure and lowest magnetic excitations in dysprosium triangles. *New J. Chem.* **2009**, *33*, 1224−1230.
(59) Chibotaru, L. F.; Ungur, L.; Aronica, C.; Elmoll, H.; Pilet, G.; Luneau, D. Structure, magnetism and theoretical study of mixed-valent $Co_3^{II}Co_4^{III}$ heptanuclear wheel: Lack of SMM behaviour despite negative magnetic anisotropy. *J. Am. Chem. Soc.* **2008**, *130*, 12445−12455.
(60) Iwahara, N.; Chibotaru, L. F. Exchange interaction between J multiplets. *Phys. Rev. B* **2015**, *91*, No. 174438.
(61) Ungur, L.; Thewissen, M.; Costes, J.-P.; Wernsdorfer, W.; Chibotaru, L. F. Interplay of Strongly Anisotropic Metal Ions in Magnetic Blocking of Complexes. *Inorg. Chem.* **2013**, *52*, 6328−6337.
(62) Krylov, D.; Velkos, G.; Chen, C.-H.; Büchner, B.; Kostanyan, A.; Greber, T.; Avdoshenko, S. M.; Popov, A. A. Magnetic hysteresis and strong ferromagnetic coupling of sulfur-bridged Dy ions in clusterfullerene $Dy_2S@C_{82}$. *Inorg. Chem. Front.* **2020**, *7*, 3521−3532.
(63) Gould, C. A.; Mu, E.; Vieru, V.; Darago, L. E.; Chakarawet, K.; Gonzalez, M. I.; Demir, S.; Long, J. R. Substituent Effects on Exchange Coupling and Magnetic Relaxation. *J. Am. Chem. Soc.* **2020**, *142*, 21197−21209.
(64) Singh, M. K.; Rajaraman, G. Acquiring a record barrier height for magnetization reversal in lanthanide encapsulated fullerene molecules using DFT and *ab initio* calculations. *Chem. Commun.* **2016**, *52*, 14047−14050.
(65) Ungur, L.; Chibotaru, L. F. Strategies toward High-Temperature Lanthanide-Based Single-Molecule Magnets. *Inorg. Chem.* **2016**, *55*, 10043−10056.
(66) Chen, C.-H.; Krylov, D. S.; Avdoshenko, S. M.; Liu, F.; Spree, L.; Yadav, R.; Alvertis, A.; Hozoi, L.; Nenkov, K.; Kostanyan, A.; Greber, T.; Woltera, A. U. B.; Popov, A. A.Selective arc-discharge synthesis of Dy_2S-clusterfullerenes and their isomer-dependent single molecule magnetism. *Chem. Sci.* **2017**, *8*, 6451−6465.
(67) Yang, W.; Velkos, G.; Liu, F.; Sudarkova, S. M.; Wang, Y.; Zhuang, J.; Zhang, H.; Li, X.; Zhang, X.; Büchner, B.; Avdoshenko, S. M.; Popov, A. A.; Chen, N. Single Molecule Magnetism with Strong Magnetic Anisotropy and Enhanced Dy•••Dy Coupling in Three Isomers of Dy-Oxide Clusterfullerene $Dy_2O@C_{82}$. *Adv. Sci.* **2019**, *6*, No. 1901352.
(68) Rinehart, J. D.; Long, J. R. Exploiting single-ion anisotropy in the design of f-element single-molecule magnets. *Chem. Sci.* **2011**, *2*, 2078−2085.
(69) Bezmelnitsyn, V.; Davis, S.; Zhou, Z. Efficient Synthesis of Endohedral Metallofullerenes in 3-Phase Arc Discharge. *Fullerenes, Nanotubes, Carbon Nanostruct.* **2015**, *23*, 612−617.
(70) Sheldrick, G. M. *SHELXT* − Integrated space-group and crystal-structure determination. *Acta Crystallogr., Sect. A: Found. Adv.* **2015**, *71*, 3−8.
(71) Sheldrick, G. M. Crystal structure refinement with *SHELXL*. *Acta Crystallogr., Sect. C: Struct. Chem.* **2015**, *71*, 3−8.
(72) CCDC-2184521 contains the supplementary crystallographic data for this paper. These data can be obtained free of charge from The Cambridge Crystallographic Data Centre via www.ccdc.cam.ac.uk/data_request/cif.

https://doi.org/10.1021/acs.inorgchem.2c04250
Inorg. Chem. 2023, 62, 5114−5122